ROYAL SOCIETY
OF CHEMISTRY

COMMUNICATION

Check for updates

Electrochemical reduction of nitrate to hydroxylamine on gold electrode†

Yangshan Xie,[a] Michiel De Ras, [iD][b] Jiwu Zhao,[cd] Tianxi Liu,[e] Feili Lai, [iD][e] Johan Hofkens [iD][bf] and Maarten B. J. Roeffaers [iD]*[a]

In this study, we explore the efficacy of gold (Au) as a selective electrocatalyst for the reduction of nitrate to hydroxylamine, a valuable nitrogen-based chemical, while also evaluating the by-product formation of ammonia. We systematically optimized various experimental parameters including nitrate concentration, pH, and applied potential. We found that at an applied potential of -0.7 V *vs.* RHE in 0.1 M HNO_3, Au achieves a 230.1 ± 19 μmol NH_2OH h^{-1} cm^{-2} yield, with a $34.2 \pm 2.8\%$ faradaic efficiency. This study underscores the potential of Au as an efficient and selective electrocatalyst for generating value-added nitrogen products through an electrochemical pathway.

Nitrogen, an element essential to all life, manifests in numerous forms, from its stable diatomic gas in the atmosphere to a myriad of nitrogen-containing molecules such as ammonia, nitrate, and organic compounds. Human activities, from industrial manufacturing to agriculture, transform these nitrogen states in ways that significantly impact the global nitrogen cycle. Such transformations—either as unintended byproducts in chemical and combustion processes or through deliberate production of fertilizers and chemicals—distort natural pathways.[1,2] Nitrate, the most oxidized form of nitrogen, is a well know pollutant in water bodies, which in excess threatens the biodiversity of ecosystems and has proven to have negative

[a] *Centre for Membrane Separations, Adsorption, Catalysis, and Spectroscopy for Sustainable Solutions, Department of Microbial and Molecular Systems, KU Leuven Celestijnenlaan 200F, 3001 Leuven, Belgium. E-mail: maarten.roeffaers@kuleuven.be*

[b] *Molecular Imaging and Photonics, Department of Chemistry, KU Leuven, Celestijnenlaan 200F, Leuven, 3001, Belgium*

[c] *State Key Laboratory of Photocatalysis on Energy and Environment, College of Chemistry, Fuzhou University, Fuzhou, 350116, China*

[d] *Division of Physical Sciences and Engineering, King Abdullah University of Science and Technology (KAUST), Thuwal, 23955–6900, Saudi Arabia*

[e] *The Key Laboratory of Synthetic and Biological Colloids, Ministry of Education, School of Chemical and Material Engineering, International Joint Research Laboratory for Nano Energy Composites, Jiangnan University, Wuxi, China*

[f] *Max Plank Institute for Polymer Research, Mainz, D-55128, Germany*

† Electronic supplementary information (ESI) available: Materials and experimental details. See DOI: https://doi.org/10.1039/d4cc03620d

health effects.[3,4] Additionally, excesses are eventually removed by natural denitrification processes, performed by microbial organisms. Due to poor selectivity, this also leads to the production of significant amounts of nitrous oxide (N_2O), a potent greenhouse gas.[5] Converting waste nitrates into valuable chemicals represents a key aspect of sustainable development and poses a significant challenge that engages engineering and research communities worldwide.

The electrochemical reduction of nitrate (NO_3RR) is gaining prominence as a method that is not only energy-efficient in producing valuable products but also environmentally beneficial for treating water pollution.[4] This process can yield a variety of nitrogen products with different oxidation states; however, research has predominantly focused on producing ammonia,[6] often overlooking the potential for selective reduction to hydroxylamine (NH_2OH). Hydroxylamine deserves further investigation due to its critical role as a precursor in the synthesis of ε-caprolactam for Nylon-6 production, which consumes more than 95% of the world's estimated production of 800 000 tons per year.[7,8] Additionally, the potential of NH_2OH as a renewable energy carrier amplifies its significance.[9,10] Traditional methods for producing NH_2OH, such as the Raschig process and catalytic hydrogenation of nitric oxide, face challenges including the use of toxic reagents such as SO_2 or NO, harsh conditions, complex processes, low conversion rates and environmental hazards.[11] Selective electrochemical NO_3RR to NH_2OH conversion presents a greener, more sustainable, cost-effective, and operationally simpler alternative. Concentrating on electrochemical routes, especially for the selective production of hydroxylamine, could drastically lower the carbon footprint as well as environmental impact of the synthesis of this key industrial chemical. This underscores the importance of targeted research into optimizing NO_3RR selectivity and efficiency. Recent studies have identified mercury as an effective electrode material for the electrochemical NO_3RR to NH_2OH.[12] However, its utility is considerably restricted due to toxicity concerns and the challenges of handling it in its liquid form. Compared to standard NO_3RR reactions performed in
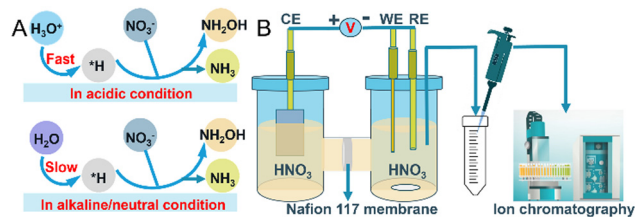
Fig. 1 (A) Pathways for surface adsorbed hydrogen, *H, generation under acidic or neutral/alkaline conditions; (B) schematic representation of the experimental approach used for the NO$_3$RR, including the H-cell configuration and ion chromatography for product analysis.

neutral conditions, which use nitrate salts and lead to the generation of stoichiometric alkali metal hydroxide byproducts, exploring the reaction in acidic nitrate conditions becomes interesting.[13–15] The increased acidity, compared to alkaline and neutral conditions, provides ample protons for sustained NO$_3^-$ hydrogenation reactions, resulting in an enhanced conversion rate of NO$_3^-$ and more energy-efficient NH$_2$OH and NH$_3$ generation (Fig. 1A).[15] The hydrogen evolution reaction (HER) inevitably competes with NO$_3$RR in acidic media. Such conditions necessitate careful electrode material selection to mitigate corrosion. Among noble metal-based electrodes, palladium generally favors NH$_3$ production,[16] while platinum is known for its efficacy in the hydrogen evolution reaction. Given these considerations, gold emerges as a particularly suitable material, noted for its durability and exceptional resistance to corrosion, even in strongly acidic conditions. This prompted our investigation into the capabilities of Au as an electrode for NO$_3$RR, particularly focusing on its selectivity for NH$_2$OH production. We rigorously tested the effects of applied potential, NO$_3^-$ concentration, and the pH of the electrolyte on the selectivity and electrochemical activity of Au towards NH$_2$OH. Our experiments revealed a significant peak faradaic efficiency (FE) of 34.2 ± 2.8% for NH$_2$OH at an applied potential of −0.7 V versus RHE in a 0.1 M HNO$_3$ solution. Notably, the NO$_3^-$ concentration was found to have a profound impact on both the yield and selectivity towards NH$_2$OH, with yields diminishing from 230.1 ± 19 μmol h^{-1} cm^{-2} in 0.1 M NO$_3^-$ to zero at 1 M KNO$_3$. Furthermore, the optimum yield of NH$_2$OH, 333 μmol h^{-1} cm^{-2}, was achieved at a pH of 0.3 in H$_2$SO$_4$ with a 0.1 M NO$_3^-$ concentration. These findings underline the potential of Au electrodes to serve as both an efficient and selective catalyst for the electrochemical reduction of NO$_3^-$ to NH$_2$OH, offering an environmentally friendly alternative to conventional production methods and mitigating associated environmental impacts.

The nitrate reduction is a complicated multi-electron, multi-proton transfer process. The electroreduction of NO$_3^-$ to NH$_2$OH involves the transfer of eight protons and six electrons. Conversely, the production of NH$_3$ from NO$_3^-$ requires ten protons and eight electrons for electroreduction. Consequently, the HER inevitably emerges as a competing reaction for NO$_3$RR in acidic media. The reactions in this work are summarized in eqn (1)–(3), where E^0 is relative to the standard hydrogen electrode (SHE):

$$NO_3^- + 8H^+ + 6e^- \rightarrow NH_3OH^+ + 2H_2O \quad E^0 = 0.73 \text{ V } vs. \text{ SHE} \tag{1}$$
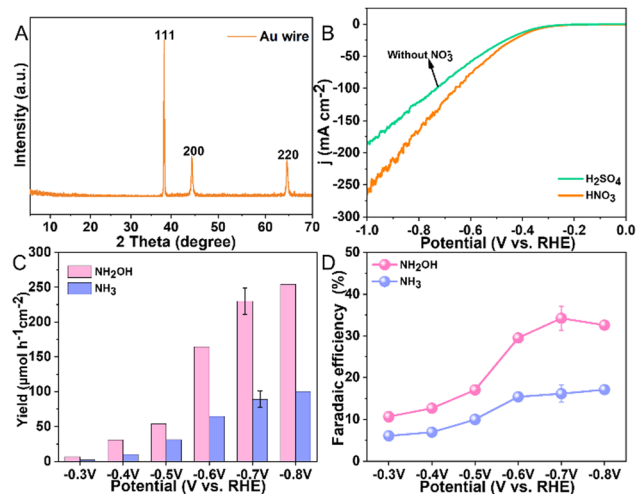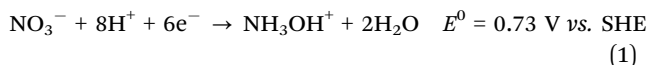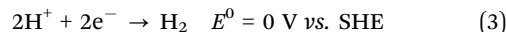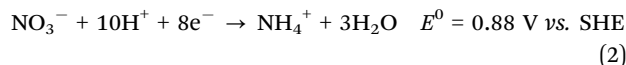

Fig. 2 Characterization and performance of a Au electrode in electrochemical NO$_3$RR: (A) XRD pattern, (B) comparative LSV curves for the Au wire electrode measured in 0.1 M HNO$_3$ and 0.1 M H$_2$SO$_4$, (C) influence of applied potential on the NO$_3$RR yield rates of NH$_2$OH and NH$_3$, and (D) faradaic efficiency integrated over 1 hour in 0.1 M HNO$_3$.

$$NO_3^- + 10H^+ + 8e^- \rightarrow NH_4^+ + 3H_2O \quad E^0 = 0.88 \text{ V } vs. \text{ SHE} \tag{2}$$

$$2H^+ + 2e^- \rightarrow H_2 \quad E^0 = 0 \text{ V } vs. \text{ SHE} \tag{3}$$

The morphology of the Au wire (diam. 0.5 mm, 99.999% pure) electrode was analyzed using scanning electron microscopy, revealing an irregular surface texture as illustrated in Fig. S1, (ESI†). Compositional analysis through energy-dispersive X-ray spectroscopy confirmed that this electrode solely exists of Au, with the detailed spectrum shown in Fig. S2, (ESI†). To ascertain the crystallinity of the electrode, X-ray diffraction was employed, with the results displayed in Fig. 2A. The recorded XRD pattern clearly exhibits the characteristic peaks of pure gold at 38.2°, 44.4°, and 65.58°. These peaks correspond to the (111), (200), and (220) crystallographic planes of Au, respectively. These results are in agreement with standard data (JCPDS 04-0784), confirming the purity of the Au wire.

We commenced our study by evaluating the electrocatalytic behavior of the Au electrode in 0.1 M HNO$_3$ and H$_2$SO$_4$ solutions, respectively, employing linear sweep voltammetry (LSV) for this characterization. This approach allowed us to assess the electrode's activity across a range of potentials from 0 V to −1 V vs. RHE (Fig. 2B). A notable increase in current density was observed beyond −0.3 V vs. RHE in 0.1 M HNO$_3$, peaking at −266 mA cm^{-2} at −1 V vs. RHE. The elevated current density in HNO$_3$, compared to that in H$_2$SO$_4$ (without NO$_3^-$), underscores the Au electrode's specific activity towards NO$_3^-$ reduction. Subsequent, our focus shifted to identifying the reaction products produced in an H-shaped three-electrode quartz cell, which was partitioned by a Nafion 117 membrane and contained 0.1 M HNO$_3$ as the electrolyte (Fig. 1B). The products of the NO$_3$RR were monitored using ion chromatography (IC), which revealed only the presence of NH$_3$ and NH$_2$OH (Fig. S3, ESI†). Subsequent experiments aimed to determine the impact of various applied potentials on the

production rates and selectivity of these identified products. By experimenting with potentials ranging from -0.3 V to -0.8 V *vs.* RHE (Fig. S4, ESI†), we observed that the yield of NH_2OH increased with more negative potentials, increasing from 6.7 µmol h^{-1} cm^{-2} at -0.3 V *vs.* RHE to 254.3 µmol h^{-1} cm^{-2} at -0.8 V *vs.* RHE (Fig. 2C). Additionally, the FE for NH_2OH production demonstrated a progressive increase from 10.6% at -0.3 V *vs.* RHE, peaking at $34.2 \pm 2.8\%$ at -0.7 V *vs.* RHE, and then slightly declining to 32.6% at -0.8 V *vs.* RHE (Fig. 2D), possibly due to the enhanced competition from the HER at these more negative potentials. The yield and FE of H_2 were determined to be 482.7 ± 40.3 µmol h^{-1} cm^{-2} and $27.1 \pm 0.9\%$ at -0.7 V *vs.* RHE, respectively (Fig. S5, ESI†). The NH_3 yield measured from UV-vis method (81 ± 10.1 µmol h^{-1} cm^{-2}) was close to IC method (89 ± 11.9 µmol h^{-1} cm^{-2}) at -0.7 V *vs.* RHE, indicative of the reliability of the determined experimental data (Fig. S6, ESI†). Notably, throughout these experiments, the yields and FE for NH_3 were consistently lower than those for NH_2OH, highlighting a pronounced selectivity towards NH_2OH production.

To examine the effect of nitrate concentration on product selectivity while maintaining a constant pH of 1, experiments were conducted at an applied potential of -0.7 V *vs.* RHE using 0.1 M HNO_3 as the electrolyte and varying concentrations of KNO_3; for the most dilute nitrate solution, a 0.05 M KNO_3 solution was used with its pH adjusted to 1 using H_2SO_4 (Fig. S7, ESI†). Fig. 3 illustrated the trends in product yield and FE with nitrate concentration at pH 1, demonstrating that the highest yield and FE of NH_2OH were achieved at a nitrate concentration of 0.1 M. At a reduced nitrate concentration of 0.05 M, the diminished adsorption of nitrate anions on the Au surface, likely slowed the NO_3RR reaction. Also at increased nitrate concentrations, a marked decline in NH_2OH yield and FE were observed. Note that, the detected hydroxylamine concentration consistently decreases over time, likely due to its oxidation by HNO_2 in acidic medium ($NH_2OH + HNO_2 \rightarrow N_2O + 2H_2O$). This was confirmed by a control experiment where KNO_2 was added to a 0.1 M HNO_3 solution containing NH_2OH. As shown in Fig. S8, (ESI†), there was a sharp drop in NH_2OH concentration following the addition. The reduced yields for both NH_2OH and NH_3 at higher nitrate concentrations are likely due to additional nitrate adsorbates obstructing the Au surface. It is assumed that adsorbed hydrogen or water is necessary for nitrate to undergo NH_3 conversion. Further analysis involved measuring the pH of the electrolyte solution post-reaction (Table S1, ESI†). Clearly, higher starting nitrate concentrations resulted in increased pH levels. Specifically, the pH increments post-reaction were ordered as follows: 0.1 M (pH = 1.30) < 0.3 M (pH = 1.73) < 0.5 M (pH = 1.96) < 0.7 M (pH = 2.20) < 1 M (pH = 2.74). The increased pH was attributed to the consumption of eight protons to produce NH_3OH^+ and ten protons to produce NH_4^+, respectively.

To investigate the effect of pH on the selectivity and yield of electrocatalytic NO_3RR over the Au electrode, we modulated the electrolyte's pH, adjusted H_2SO_4 while keeping 0.1 M KNO_3 constant, and applied a potential of -0.7 V *vs.* RHE for 1 hour (Fig. S9, ESI†). Fig. 4A and B and Fig. S10 (ESI†) illustrated that the selectivity and yield of NH_2OH and NH_3 significantly
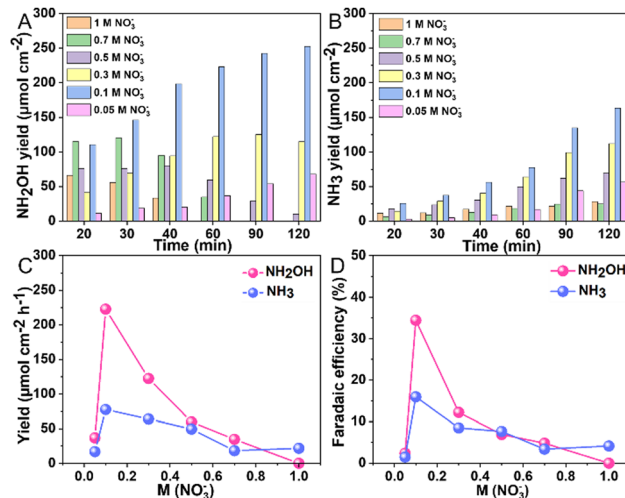

Fig. 3 Variation in NH_2OH (A) and NH_3 (B) yield rates across different nitrate concentrations at pH 1; performance assessed at an applied potential of -0.7 V *vs.* RHE over a 2-hour reaction time; (C) yield rates and (D) faradaic efficiency of NH_2OH and NH_3 across different nitrate concentrations at pH 1 with an applied potential of -0.7 V *vs.* RHE for a duration of 1 hour.

depended on the acidity of the solution, particularly at pH values below 0.5. The yield of NH_2OH notably increased from 63.5 µmol h^{-1} cm^{-2} at pH 2 to 333.1 µmol h^{-1} cm^{-2} at pH 0.3, but then decreased to 146.6 µmol h^{-1} cm^{-2} at pH 0. Meanwhile, the yield of NH_3 consistently rose at lower electrolyte pH levels, with a significant uptick observed within the pH range of 0 to 0.5, culminating in a yield of 792.5 µmol h^{-1} cm^{-2} at pH 0. These data highlight the substantial impact of acidity on the
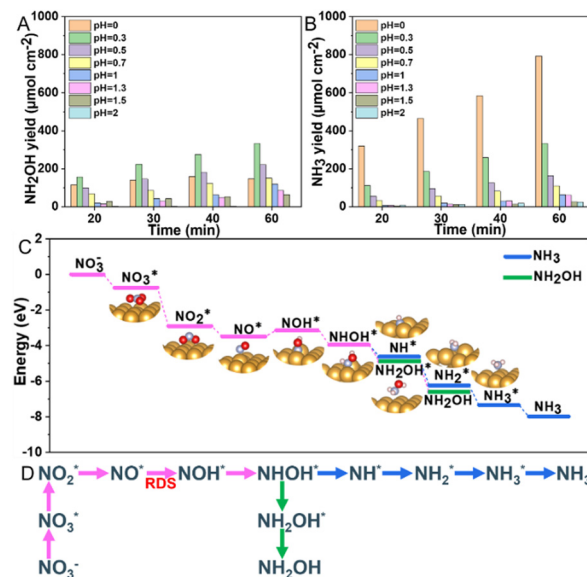

Fig. 4 Yield rates of NH_2OH (A) and NH_3 (B) across various pH levels, assessed in a solution of 0.1 M KNO_3 with H_2SO_4 adjusting the pH, at an applied potential of -0.7 V *vs.* RHE for a period of 1 hour; (C) the Gibbs free energy diagram for NO_3RR on Au wire; (D) the possible NO_3RR pathway on the Au electrode.

performance and selectivity of the Au electrode in the reduction of nitrate. At more acidic conditions, there is an increased proton availability facilitating the reaction outlined in eqn (1) and (2) for NH_2OH and NH_3 production. However, this also favors the competing HER.

To evaluate the stability of the Au wire, five consecutive cycles were performed in 0.1 M HNO_3 at -0.7 V vs. RHE, with each cycle lasting 1 hour. The consistent NH_2OH yield rate and FE observed indicate the favorable stability of the Au electrode under these conditions (Fig. S11, ESI†). SEM analysis of the Au wire after reaction showed preserved surface microstructure, with no apparent damage observed (Fig. S12, ESI†). Furthermore, also the XRD patterns remained unchanged (Fig. S13, ESI†). The current response results from LSV remained similar except for a slight increase (Fig. S14, ESI†), which may be attributed to the improved activation of the catalyst. Elemental analysis via inductively coupled plasma mass spectrometry (ICP-MS) analysis evidenced that there was no detectable Au^{3+} leaching in the electrolyte after reaction (Table S2, ESI†). These results demonstrated that Au wire serves as a robust catalyst under acidic conditions for the NO_3RR conversion to NH_2OH and NH_3.

To elucidate the mechanism of nitrate reduction on Au wire, density functional theory (DFT) calculations on Au (111) facet were performed. Fig. 4C details these simulations, which begins with the spontaneous adsorption of nitrate onto the Au electrode surface, marked by a favorable Gibbs free energy change of -0.75 eV. The reduction sequence involves adsorbed nitrate (NO_3^*) being reduced to adsorbed nitrite (NO_2^*) which is then converted to NO^*. The subsequent step involves the reduction of this adsorbed nitric oxide to hydroxylamine oxime (NOH^*), identified as the rate-determining step (RDS) in this pathway, requiring an energy of 0.35 eV. NOH^* is then further reduced to $NHOH^*$, NH_2OH^* and finally NH_2OH desorbs. Conversely, the formation of NH_3 from $NHOH^*$ involves multiple steps beginning with $NHOH^*$ first converting to NH^*, followed by NH_2^*, then to NH_3^* before NH_3^* desorbs to produce NH_3 (Fig. 4D and Fig. S15, ESI†). The lower Gibbs free energies of the formation and the desorption of NH_2OH^* indicate it occurs spontaneously, inherently favoring the formation of NH_2OH (Table S3, ESI†). The relatively simplicity of the NH_2OH pathway, compared to the multi-step process required for NH_3 formation, predominantly drives the selective formation of NH_2OH. The energy barrier of the RDS from Au (0.35 eV) is lower than that of other reported catalysts, such as Ni (0.37 eV),[17] Rh (0.39 eV),[17] Pd (0.72 eV),[17] PdFe (0.74 eV),[18] Cu/Cu_2O (0.84 eV)[19] and $Fe_3C–Cu_3$ (1.28 eV)[20] (Table S4, ESI†).

In summary, this study establishes Au as a highly effective electrocatalyst for the selective NO_3^- reduction to NH_2OH. Through meticulous experimentation involving electrolyte composition, nitrate concentration, pH and applied potential, we achieved an NH_2OH yield of 230.1 ± 19 μmol h^{-1} cm^{-2} under optimal conditions. This performance is notably exceeding the yields commonly reported in the literature and achieves a faradaic efficiency of $34.2 \pm 2.8\%$ at -0.7 V vs. RHE, setting a new benchmark in electrochemical nitrate reduction. This study provides an understanding of the electrolyte engineering of nitrate solutions and may motivate further studies into gold or other materials to selectively generate NH_2OH and other products from waste nitrates.

Data availability

The data supporting this article have been included as part of ESI.†

Conflicts of interest

There are no conflicts to declare.

Notes and references

1 G. Qing, R. Ghazfar, S. T. Jackowski, F. Habibzadeh, M. M. Ashtiani, C. P. Chen, M. R. Smith, 3rd and T. W. Hamann, Chem. Rev., 2020, 120, 5437–5516.
2 V. Rosca, M. Duca, M. T. de Groot and M. T. M. Koper, Chem. Rev., 2009, 109, 2209–2244.
3 S. Garcia-Segura, M. Lanzarini-Lopes, K. Hristovski and P. Westerhoff, Appl. Catal., B, 2018, 236, 546–568.
4 H. Xu, Y. Ma, J. Chen, W.-X. Zhang and J. Yang, Chem. Soc. Rev., 2022, 51, 2710–2758.
5 Y. Zeng, C. Priest, G. Wang and G. Wu, Small Methods, 2020, 4, 2000672.
6 A. Adalder, S. Paul, N. Barman, A. Bera, S. Sarkar, N. Mukherjee, R. Thapa and U. K. Ghorai, ACS Catal., 2023, 13, 13516–13527.
7 W. Lewdorowicz, W. Tokarz, P. Piela and P. K. Wrona, J. New Mater. Electrochem. Syst., 2006, 9, 339–343.
8 J. Ritz, H. Fuchs and H. G. Perryman, Ulmann's Encyclopedia of Industrial Chemistry, 2000, DOI: 10.1002/14356007.a13_527.
9 S. Jia, L. Wu, X. Tan, J. Feng, X. Ma, L. Zhang, X. Song, L. Xu, Q. Zhu, X. Kang, X. Sun and B. Han, J. Am. Chem. Soc., 2024, 146, 10934–10942.
10 D. H. Kim, S. Ringe, H. Kim, S. Kim, B. Kim, G. Bae, H.-S. Oh, F. Jaouen, W. Kim, H. Kim and C. H. Choi, Nat. Commun., 2021, 12, 1856.
11 X. Kong, J. Ni, Z. Song, Z. Yang, J. Zheng, Z. Xu, L. Qin, H. Li, Z. Geng and J. Zeng, Nat. Sustainability, 2024, 7, 652–660.
12 I. Taniguchi, N. Nakashima, K. Matsushita and K. Yasukouchi, J. Electroanal. Chem. Interfac. Electrochem., 1987, 224, 199–209.
13 J. Shen, Y. Y. Birdja and M. T. M. Koper, Langmuir, 2015, 31, 8495–8501.
14 Y. Lv, S.-W. Ke, Y. Gu, B. Tian, L. Tang, P. Ran, Y. Zhao, J. Ma, J.-L. Zuo and M. Ding, Angew. Chem., Int. Ed., 2023, 62, e202305246.
15 R. Zhang, C. Li, H. Cui, Y. Wang, S. Zhang, P. Li, Y. Hou, Y. Guo, G. Liang, Z. Huang, C. Peng and C. Zhi, Nat. Commun., 2023, 14, 8036.
16 J. Lim, C.-Y. Liu, J. Park, Y.-H. Liu, T. P. Senftle, S. W. Lee and M. C. Hatzell, ACS Catal., 2021, 11, 7568–7577.
17 M. Karamad, T. J. Goncalves, S. Jimenez-Villegas, I. D. Gates and S. Siahrostami, Faraday Discuss., 2023, 243, 502–519.
18 Y. Zhou, L. Zhang, Z. Zhu, M. Wang, N. Li, T. Qian, C. Yan and J. Lu, Angew. Chem., Int. Ed., 2024, 63, e202319029.
19 N. Zhou, Z. Wang, N. Zhang, D. Bao, H. Zhong and X. Zhang, ACS Catal., 2023, 13, 7529–7537.
20 Y. Hua, N. Song, Z. Wu, Y. Lan, H. Luo, Q. Song and J. Yang, Adv. Funct. Mater., 2024, 34, 2314461.